2.3 NUMERICAL SIMULATION OF AIRBORNE CLOUD SEEDING FOR THE DAPHNE PRECIPITATION ENHANCEMENT PROJECT IN CENTRAL GREECE

Dimitrios Bampzelis[1]*, Vlado Spiridonov[2], Stergios Kartsios[1], Ioannis Pytharoulis[1], Ioannis Tegoulias[1] and Theodore Karacostas[1].

1. Department of Meteorology and Climatology, School of Geology, Faculty of Sciences, Aristotle University of Thessaloniki, 541 24, Thessaloniki, Greece
2. Faculty of Natural Sciences and Mathematics, Institute of Physics, Gazi Baba bb 1000 Skopje.

1. INTRODUCTION

One of the most crucial and difficult part in cloud seeding operations is how to determine the right seeding location, amount and time in order to maximize seeding effects. This study uses a 3D cloud-resolving model with AgI seeding process to simulate AgI seeding by aircraft, according to the seeding methodology, seeding hypothesis and seeding rates, adopted. The analyses are performed in order to verify and document the ability of the cloud model to: a) simulate the initiation, growth and behavior of such storms and b) to evaluate the effects of seeding with respect to rainfall increase. This research work is part of the DAPHNE project, aiming at drought mitigation for the area of Thessaly in central Greece, applying airborne cloud seeding techniques for rain enhancement during the warm season of the year.

Thessaly (Fig. 1b) is located in the eastern part of central Greece covering about 13.700km^2 with elevation ranging from sea level up to 2.800m. Precipitation regime of the area is the typical Mediterranean regime (wet winters, dry summers) exhibiting high inter-annual variation due to the atmospheric circulation from west to east. Thus, mean annual precipitation in the western mountainous areas exceeds 2.000mm, while central and eastern plain areas receive only 420mm (Flocas, 1994). Although the eastern plain area is characterized by semi-arid conditions, is one of the most agricultural productive regions of Greece producing cotton, wheat, maize, apples, olives and many more. The increased agricultural activities, the intensified agricultural practices applied, the oversized pumping of underground water and the bad management of irrigation water has led to significant degradation of the water resources in the area.

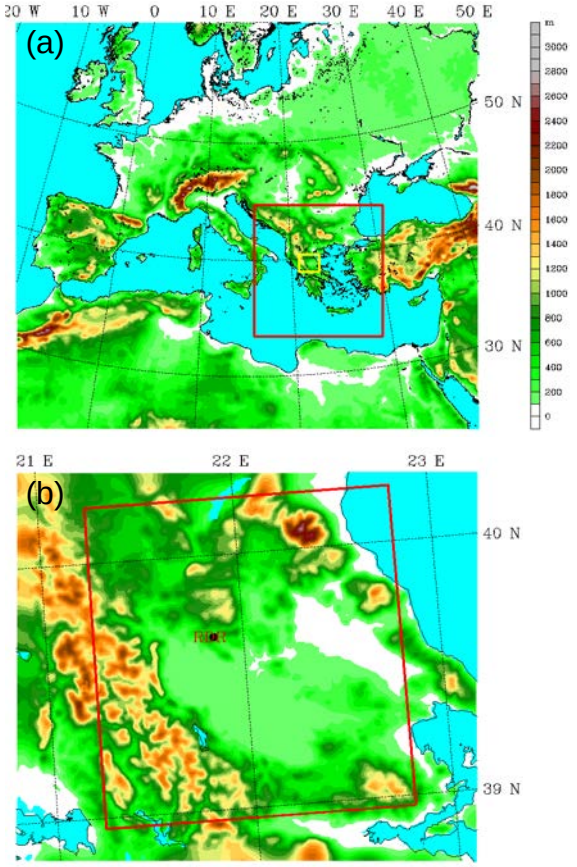

Fig. 1. The topography of: (a) Domain01 (D01) used by WRF-ARW with embedded domains D02 (red frame) and D03 (yellow frame) and (b) Domain03 (D03) nest. RDR denotes the location of the weather radar while the red frame over Thessaly encompasses the region with radar data.

Synoptic classification analysis over the area (Bampzelis and Karacostas, 2014) for the warm season (April – September) indicated 7 storm

*Corresponding author address: Dr. Dimitrios Bampzelis, Dept of Meteorology and Climatology, School of Geology, Faculty of Sciences, Aristotle Univ. of Thessaloniki, 54124 Thessaloniki, Greece; e-mail: babzel@geo.auth.gr

producing synoptic situations mainly associated with the passage of troughs. Among them, northwest (NW) and southwest (SW) flow are the most frequently observed synoptic situations having 32% and 18% of appearance. Two selected case studies, one of each aforementioned synoptic situation, were chosen for the analysis. Studies of convective activity over the area (Bampzelis and Karacostas 2012) revealed that cells developing under SW synoptic situation exhibit earlier initiation within the day, higher speeds, lower reflectivity values and lower tops compared with cells developing under NW synoptic situation. They also tend to form in greater numbers creating multicell complexes of storms but, in most cases, do not reach intense characteristics.

The WRF model (WRF-ARW ver 3.5.1) is applied to simulate the airflow characteristics of the convective activity. Simulated soundings, derived from the WRF outputs, are used to initialize the convective cloud model. Storm characteristics are observed using a C-band weather radar and the cell tracker TITAN (Thunderstorm Identification, Tracking, Analysis, and Nowcasting).

Previous studies using the high resolution cloud-resolving model have shown that the model is capable of representing the storm structure and kinematics, such as radar reflectivity, wind speed and direction and seeding agent dispersion.

2. METHODOLOGY

The nonhydrostatic WRF-ARW model (Skamarock et al. 2008, Wang et al. 2013) is engaged to simulate the sounding that will be used as input to the cloud model at time and place where the actual storms developed within the area of interest for a more realistic storm depiction. Three model domains are employed using 2-way telescoping nesting covering Europe-Mediterranean sea and northern Africa (D01), the wider area of Greece (D02; Fig. 1a) and central Greece- Thessaly region (D03; Fig. 1b) at horizontal grid-spacing of 15km, 5km and 1km respectively. The model uses ECMWF operational analyses at 6-hourly intervals (0.25°x0.25° lat.-lon.) as initial and boundary conditions of the coarse domain.

Storms are observed and recorded using a C-band (5cm) weather radar, being located within domain three (D03; Fig. 1b) (39.674N, 21.837E), and TITAN algorithm (Dixon and Wiener, 1993). Radar reflectivity measurements have approximately 750x750m spatial and 3.5min temporal resolution.

The 3D cloud model (Spiridonov and Curic, 2006) is a three-dimensional, non-hydrostatic, time-dependant, compressible system, which is based on the Klemp and Wilhelmson (1978) dynamics, the bulk cloud microphysics scheme from Lin et al. (1983) that takes into account 6 water variables (water vapor, cloud droplets, ice crystals, rain, snow and graupel) and Orville and Kopp (1977) thermodynamics. The bulk microphysical parameterization uses a double-moment scheme for all species. The activation of AgI is parameterized by the three nucleation mechanisms based on Hsie (1980) and Kopp (1988) and the calculation of agent dispersion is done using an additional conservation equation. The dispersion of the agent takes place on a sub-grid scale while the advection and diffusion are represented by individual puffs spreading in time according to the turbulent diffusion coefficients proposed by Georgopoulos and Seinfeld (1986). The equivalent radar reflectivity factors for hail and rain are computed according the equations given by Smith et al. (1975) and the empirical equation for snow by Sekhon and Srivastava (1970). More detail information about the model, initial and boundary conditions, numerical technique and initialization could be found in Telenta and Aleksic (1988), Spiridonov and Curic (2006), Barth et al. (2007) and Spiridonov et al. (2014).

The initial conditions applied within the model come from the WRF simulated sounding over the area of interest. Initial impulse for convection is an ellipsoidal warm bubble with maximum temperature perturbation in the bubble center. The model domain has dimensions of $60x60x20km^3$. The spatial grid resolution is $500x500x250m^3$ and the temporal resolution for integration is 5s and 10s, plus a smaller one of 1s and 2s, for solving sound waves.

3. RESULTS

Three-dimensional numerical simulations are performed to analyze the ability of the model to simulate storm initiation, development and characteristics as well as to investigate aircraft seeding by silver iodide of two subjectively selected cases.

3.1 Case 1 (07/07/2012 - Northwest flow)

Surface analysis during the occurrence of the event reveals the absence of any weather system activity. A weak low pressure area situated to the east establishes light surface winds from northerly directions, altered to southeast during noon time near surface layer, by the strengthening of the sea breeze. In the middle troposphere (500hPa) a ridge is observed a few degrees to the west of the area associated with a low pressure system to the northeast, establishing a northwest flow over the area of interest. The combination of the observed divergence in the upper troposphere (300hPa) with convergence in the lower (700 and 850hPa), promotes the ascending motion of the lower tropospheric air masses, triggering convection appearance. Convection is also favoured by the presence of thermodynamic instability related to moisture availability and vertical lapse rate.

The skew-T/logP diagram of the sounding which is derived from WRF over the area at the time when the actual storms appeared indicates the presence of low-level moisture, weak wind shear and veering in the layer between 800hPa and 400hPa. The Convective Available Potential Energy is 752(J/Kg), the Severe Weather Treat Index is 180 and the bulk Richardson number is 95 supporting multicell or singlecell formation. K index is 38,5, Showalter index is -1,2 and Lifted index -2,5 indicating strong, moderate and weak convective activity respectively.

The radar observed convective activity appeared at about 13:30UTC lasting for three hours until 16:30 in which several cells formed over the area of interest. Cells exhibited mean max reflectivities of 54.2dBz, mean max tops at 8.8Km, mean duration of 1.2 hours and mean volume about 217Km^3. The mean direction of movement is from northwest to southeast (152^o) with an average speed of 15.1Km/hr following the mean tropospheric wind. Mean precipitation rate is 16.8mm/hr while mean Vertical Integrated Liquid is 19.8Kgr/m^2.

Modelled simulation of the convective case shows the development and evolution of a typical singlecell storm. The simulated life cycle and direction of movement of the storm are similar. Modelled reflectivity values coincide with observed ones.

Seeding takes place 25 minutes from simulation start at height 4.75km on the upwind side of storm movement from NW to SE (from x: 30 to 36 km and y: 22 to 26 km, at 90^o-180^o angle). The seeding rate is 2.5 g/s. The AgI aircraft seeding trajectory is well seen in the horizontal cross section plot shown in Fig. 2. Seeding material is correctly introduced at the cloud side, in the main inflow area, in radar reflectivity zone greater than 35 dBz between -6^{o}C and -8^{o}C.

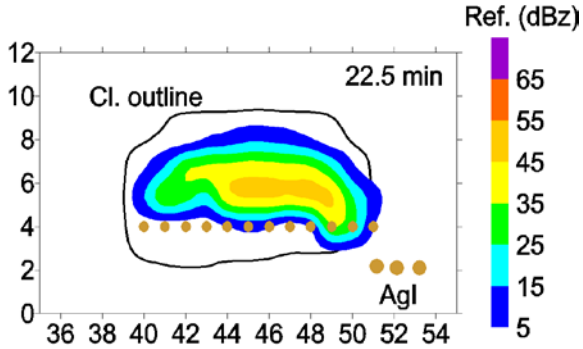

Fig. 2. Horizontal cross section (PPI plots) at height 4.75km, 25 minutes from simulation start showing seeding placement on the upwind side of storm movement from NW to SE.

The effects of seeding could be identified by comparing the radar reflectivity (horizontal and vertical transects) between both cases in different simulation times. Observed and modeled vertical cross sections (RHI plots) of the reflectivity along SW to NE direction for both unseeded and seeded case are depicted in Fig. 3. Initial differences between seeded and unseeded cell appear approximately 8 minutes after the seeding operation.

A slight difference in reflectivity echoes between unseeded and seeded case is noted a few minutes after the seeding. The area that reflectivity exceeds 55 dBz, is slightly larger reaching up to 8Km assuming an updraft enhancement. The difference is also evident in the cloud mature stage, when intensive rainfall occurs.

A more realistic view of the storm is given through a three-dimensional depiction of the cloud shown in Fig. 4, viewed from the southeast (SE). Hydrometeors (cloud water, cloud ice, hail, rain and snow), expressed through their mixing ratios at 50 minutes from simulation start. The plot size dimensions of AgI have been increased for visualization purposes. It is well seen how seeding material is released in the appropriate place in the inflow region (see blue fields), within the storm's area, during the growing phase. The cloud grows quite rapidly and the upper portion

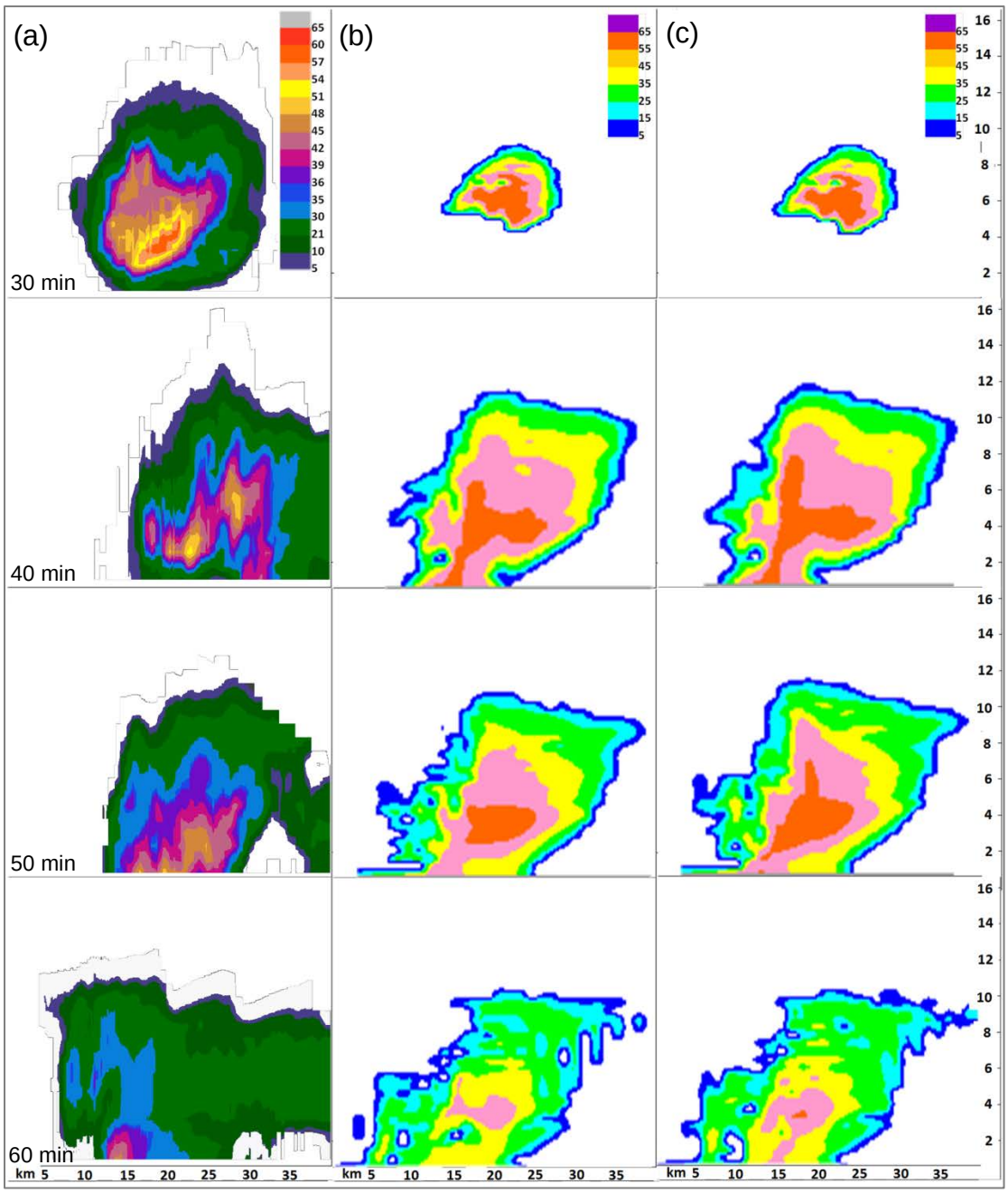

Fig. 3. Radar observed and modeled simulated vertical cross sections (RHI plots) of reflectivity along SE to NW direction from 30 to 60 minutes, at 10 min intervals (a):observed, (b): unseeded and (c):seeded.

extends towards SW, 10 min after the seeding. The time evolution of reflectivity values between observed, unseeded run and seeded run can be seen in Fig. 5a. In order to evaluate the seeding effects the evolution of cloud water content, expressed in gr/m^3 is depicted for the unseeded and seeded numerical simulations in Fig. 5b. It is evident that cloud water content, for the seeded case, is rapidly decreases after seeding as a result of AgI activation which changes the content of water substance to ice, increasing the number of ice concentration in the cloud. Although microphysical changes within the cloud are visible, as a result of seeding, the primary concern should be precipitation enhancement at the ground. Fig. 5c displays the time evolution of total precipitation for both unseeded and seeded cases. As it is seen precipitation increase is estimated at 33.9%.

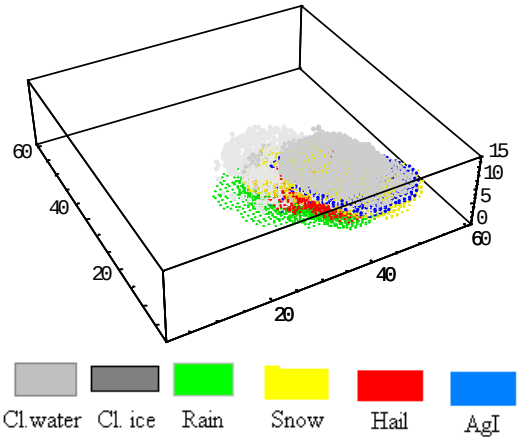

Fig. 4. 3D capture of the cloud, as seen from the SW at 50 min. from simulation start.

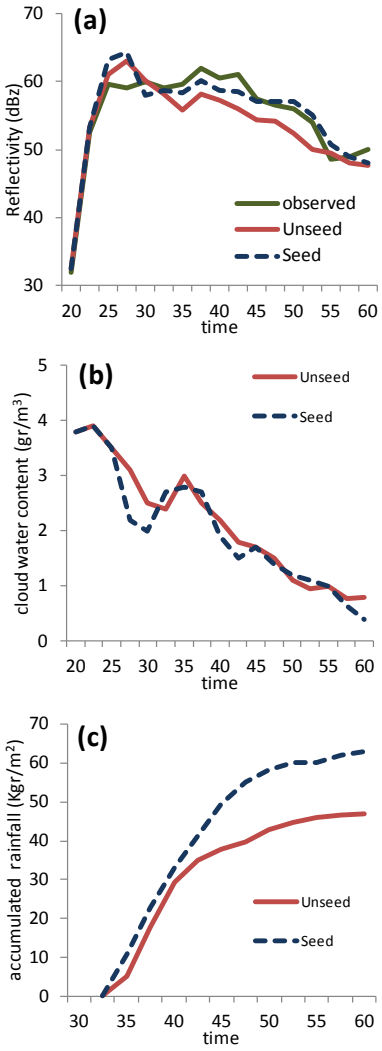

Fig. 5. Time evolution of: (a) reflectivity values, (b): water content and (c) accumulated precipitation of the unseeded and the seeded cloud.

3.2 Case 2. (29/06/2013 Southwest flow)

Surface analysis chart during the event shows no significant activity, like most of normal summer days over the area. The pattern depicts a weak low pressure to the east. Light surface winds from southwest direction are observed during the event. In the middle troposphere (500 hPa) a trough is observed, with its axis located to the west of the area of interest. Upward motions are favored downstream of the trough (that is on its eastern flank), due to positive vorticity advection. The trough is extended all the way to the upper troposphere (300 hPa), being associated with divergence over the area of interest. Convergence is observed in the lower troposphere, 700hPa and 850hPa. The combination of these promotes the ascending motion of lower tropospheric air masses. The skew-T/logP diagram of the sounding, also derived from WRF over the area at the time when the actual storms appeared, indicates the presence of low-level moisture at 700hPa and weak wind shear between 800hPa and 600hPa. Instability indices derived from the sounding, in general, indicate weak convection activity. The Severe Weather Treat Index is 61, K index is 25.7, Showalter index is 3 and Lifted index 1.2 indicating no and weak convective activity.

The radar observed convective activity appeared at about 11:15UTC lasting for five hours, in which several cells formed over the area of interest. Cells exhibited mean max reflectivities of 50.2dBz, tops at 6.7Km, mean duration of half an hour and volume about 70Km^3. The mean direction of movement is from southwest to northeast (35^o) with an average speed of 21Km/hr. The mean precipitation rate is 14.7mm/hr while the mean Vertical Integrated Liquid is 19.9Kgr/m^2.

As in case 1, the cloud model adequately simulated cell development, direction of movement and reflectivity values. The optimum seeding approach followed was seeding at 15 minutes from simulation start, at height 4.25km on the upwind side of storm movement with a seeding rate of 20 g/s. Seeding material is correctly introduced at the cloud side, in the main inflow area.

Small differences in reflectivity echoes between unseeded and seeded case are observed a few minutes after seeding and are maximized during the clouds mature stage, when most rainfall occurs.

The time evolution of reflectivity values between observed, unseeded and seeded run, as well as cloud water content and total precipitation are depicted in Fig. 6. Estimated accumulated precipitation increase is 48% Fig 6c).

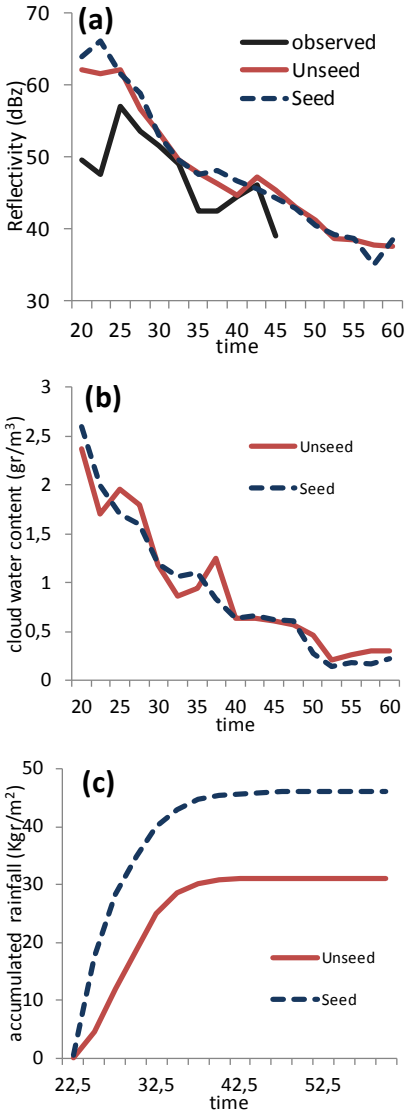

Fig. 6. Time evolution of: (a) reflectivity values, (b): water content and (c) accumulated precipitation of the unseeded and the seeded cloud for case 2.

4. CONCLUSIONS

Effective cloud seeding for rain enhancement should be conducted following an optimal seeding method including right seeding location, time and amount. Modeling of the seeding procedure is a valuable tool at investigating responses on cloud dynamical and microphysical features. Moreover precipitation enhancement can be measured and tested against different seeding methods, rates and locations.

Although both cases selected for this study are subjectively selected, the greatest efficiency is achieved if seeding material is properly placed along the cloud base at strong updraft area during the cloud's developing stage. Seeding optimization is achieved combining thermodynamic characteristics of the atmosphere as well as reflectivity values from the weather radar. Results show that cloud microphysical characteristics altered since seeded clouds exhibit earlier development of precipitation, a slight enhancement of the updraft and rainfall increase in the order of 30% to 40%. AgI particles acts as cloud ice forming since cloud ice mixing ratio increases after seeding as a result of AgI particles activation, which change the contents of water substance and increase of ice concentration in the cloud. Rainwater mixing ratio is also increased and the cloud water mixing ratio along with hail are decreased.

Results emphasize the strong interaction between cloud dynamics and microphysics, especially in small scale processes, which influence seeding agent transport and diffusion within the storm's complex environment. Seeding effects are strongly depended upon the seeding strategy, relying on the exact seeding time, the right placement of the seeding agent and the appropriate seeding rate.

This paper demonstrates modeling techniques applied so far within the context of the ongoing project. Near future activities include real seeding trials that will be used to evaluate modeling results and to explore further possibilities on rain enhancement over the area via cloud seeding.

5. REFERENCES

Bampzelis, D., Karacostas, T., 2012: Radar derived storm characteristics over central Greece., *Advances in Meteorology, Climatology and Atmospheric Physics, Springer Atmospheric Sciences*, 27-33, DOI 10.1007/978-3-642-29172-2_5.

Bampzelis, D., Karacostas, T., 2014: Radar storm characteristics based upon their synoptic situations over Thessaly. *Proc. 12th Int. Conf. of Meteorology, Climatology and Physics of the Atmosphere.* Heraklion, Greece, 28-31 May, Vol. 1, 117-121.

Barth, M.C., Kim, S-W., Wang, C., Pickering, K. E., Ott, L. E., Stenchikov, G., Leriche, M., Cautenet, S., Pinty, J-P., Barthe, Ch., Mari, C., Helsdon, J. H., Farley, R. D., Fridlind, A. M., Ackerman, A. S., Spiridonov V., Telenta B., 2007: Cloud-scale model intercomparison of chemical constituent transport in deep convection, *Atmos. Chem. Phys. 7*, 4709–4731.

Dixon, M. J., Wiener, G., 1993: TITAN: Thunderstorm Identification, Tracking, Analysis and Nowcasting: A Radar-based Methodology. *J. Atmos. and Oceanic Technol.*, 10, 6, 785-797.

Flokas, A.A., 1994: Meteorology and Climatology Courses, *Ziti Publishing*, Thessaloniki, 465pp (in Greek).

Georgopoulos, P.G., Seinfeld, J.H., 1986: Mathematical modeling of turbulent reacting plumes – general theory and model formulation*. Atmos Environ 20*, 1791–1802.

Hsie, E.Y., Farley, R.D., Orville, H.D., 1980: Numerical simulation of ice-phase convective cloud seeding. *J Appl Meteorol* 19, 950–977.

Kopp, F.J., 1988: A simulation of Alberta cumulus. *J Appl Meteorol 27*, 626–641.

Lin, Y-L., Rarley, R.D., Orville, H.D., 1983. Bulk parameterization of the snow field in a cloud model. *J Appl Meteorol 22*, 1065–1092.

Orville, H.D., Kopp, F.J., 1977: Numerical simulation of the history of a hailstorm. *J Atmos Sci. 34*, 1596–1618.

Sekhon, R.S., Srivastava, R.C., 1970: Snow size spectra and radar reflectivity. *J. Atmos. Sci., 27,* 299-307.

Skamarock, W.C., Klemp.,J.B., Dudhia, J., Gill, D.O., Barker, D.M., Duda, M.G., Huang, X-Y., Wang, W., Powers, J.G., 2008: A description of the Advanced Research WRF Version 3. NCAR/TN-475.

Smith, P.L., Myers, G.G., Orville, H.D., 1975: Radar reflectivity calculations on numerical cloud models using bulk parameterization of precipitation. *J. Appl. Meteor., 14*, 1156-1165.

Spiridonov, V., Curic, M., 2006: A three-dimensional modeling studies of hailstorm seeding*. J Weather Modif*. 38, 31–37.

Spiridonov, V., Karacostas, T., Bampzelis, D., Pytharoulis, I., 2015: Numerical Simulation of Airborne Cloud Seeding over Greece, Using a Convective Cloud Model, Asia-Pac. J. Atmos. Sci., 51(1), 1-17*.*

Telenta, B., Aleksic, N., 1988: A three-dimensional simulation of the 17 June 1978 HIPLEX case with observed ice multiplication. *2nd International cloud modeling workshop, Toulouse, 8–12 August 1988*. WMO/TD No. 268, 277–285.

Wang, W., Bruyère, C., Duda, M., Dudhia, J., Gill, Kavulich, M., Keene, K., Lin, H-C., Michalakes, J., Rizvi, S., Zhang, X., Beezley, J., Coen, J., Mandel, J., 2014: *ARW Version 3 Modeling System User's Guide. NCARMMM.* pp. 423.

Acknowledgments: *This research work is part of DAPHNE project (11SYN_8_1088_TPE) which is co-funded by the European Union (European Regional Development Fund) and Greek National Funds, through the action "COOPERATION 2011: Partnerships of Production and Research Institutions in Focused Research and Technology Sectors" in the framework of the operational programme "Competitiveness and Enterpreneurship" and Regions in Transition (OPC II, NSRF 2007-2013).*